Supplementary Material

High-Efficiency Photoacoustic Transducers Based on Plasmonic EGaIn Liquid Metal Nanoparticle

Cheng Luo, Rui Zhou, Yihao Li, Min Li, Xiaoyan Wen, Ming-Yu Li, Shuo Deng and Sisi Liu, Hongyun Gao*, Haifei Lu*

School of Physics and Mechanics, Wuhan University of Technology, Wuhan 430070, China.

ccyun@126.com, haifeilv@whut.edu.cn

Photoacoustic characterization system

Fig. S1 presents a schematic diagram of the experimental setup used for photoacoustic characterization in this study.

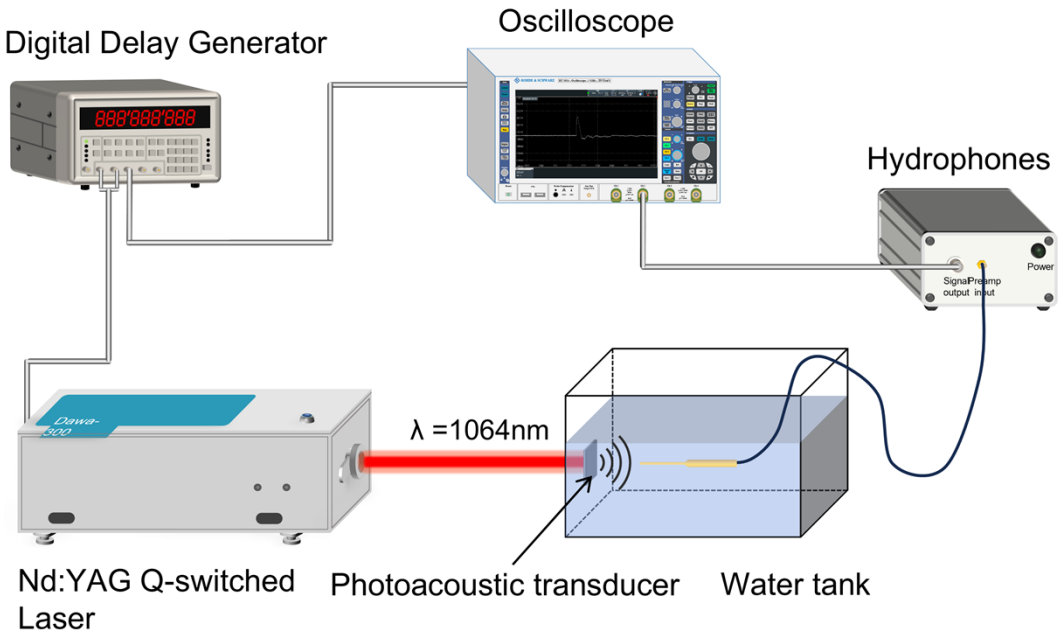

Figure S1 Schematic diagram of the photoacoustic characterization system.

Simulation of different metal nanoparticle

Fig. S2 shows the simulated electric field distribution for three types of metal nanoparticles (diameter: 300 nm) at an excitation wavelength of 1064 nm. The results indicate that the EGaIn nanoparticles exhibit slightly stronger surface plasmon resonance (SPR) at 1064 nm compared to traditional noble

metal nanoparticles.

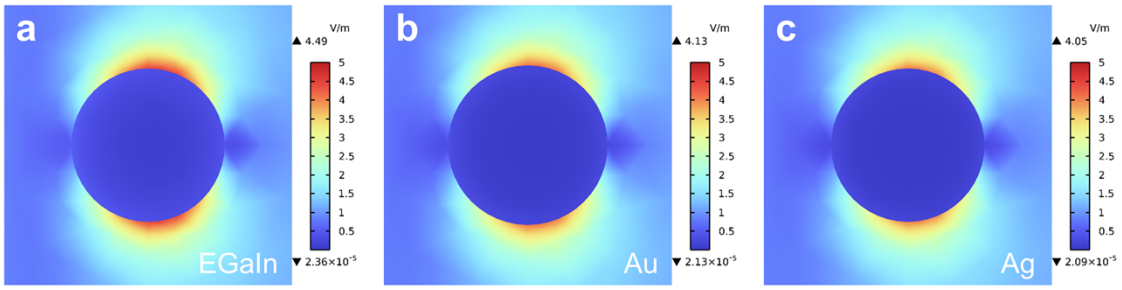

Figure S2 Simulated electric field distribution for different metal nanoparticles at 1064 nm.

Simulation of different metal nanoparticle-Scattering&Extinction&Absorption

Figure S3 displays the simulated absorption, scattering, and extinction spectra of various metallic nanoparticles. The results indicate that increasing nanoparticle size induces a redshift in the absorption spectrum, as demonstrated in Figure S8(d) for EGaIn. While gold and silver exhibit stronger absorption in the visible range, EGaIn achieves significantly higher absorption efficiency at the targeted 1064 nm wavelength discussed in this work. This superior performance at 1064 nm underscores the rationale for selecting EGaIn in this work's proposed application.

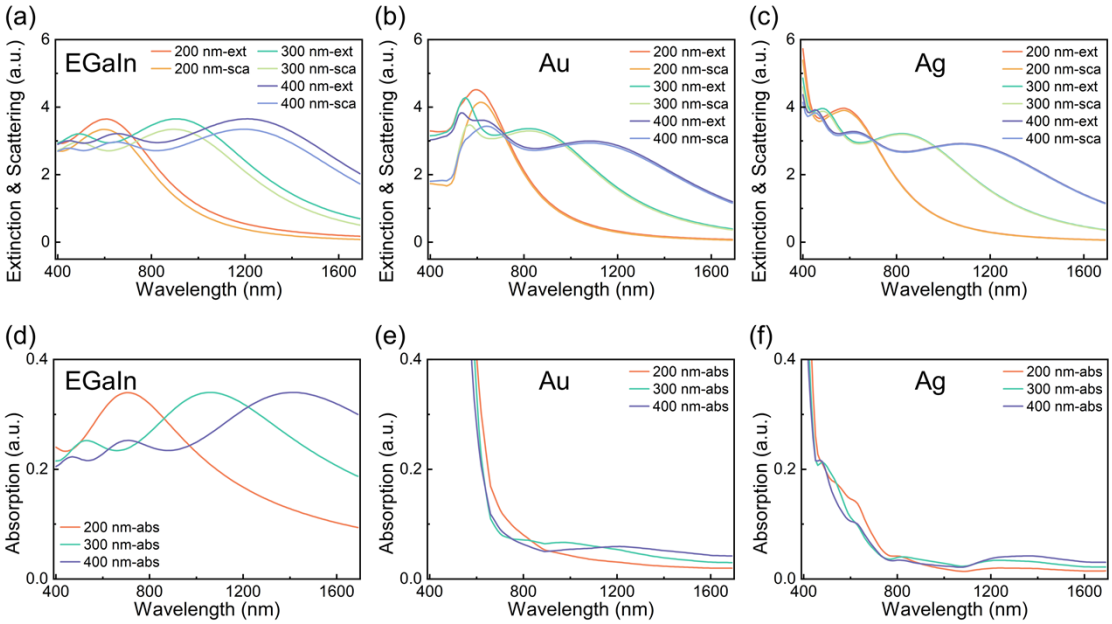

Figure S3 Simulation results of scattering (sca), extinction (ext) and absorption (abs) of different metal nanoparticles. (a)EGaIn; (b) Au; (c) Ag; (d)EGaIn; (e) Au; (f) Ag

EDS mapping results of LMNPs

Fig. S4 presents the energy-dispersive X-ray spectroscopy (EDS) mapping results of the liquid metal nanoparticles (LMNPs). The higher density of sulfur (S) on the nanoparticles compared to the surrounding area confirms that MPTMS (3-Mercaptopropyltrimethoxysilane) acts as a stabilizer during nanoparticle preparation. The binding of MPTMS to the LMNP surface effectively stabilizes the nanoparticles.

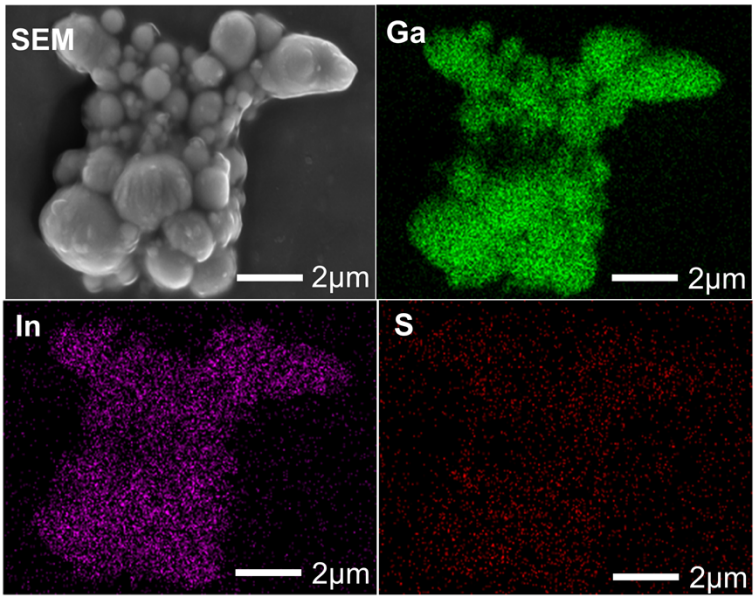

Figure S4 EDS mapping of LMNPs.

SEM image of cross-section of EGaIn/PDMS-based photoacoustic transducer

Figure S5 demonstrates the SEM image of the cross-section of the EGaIn/PDMS-based photoacoustic transducer with a thickness of about 120 μm, which shows a uniform particle distribution.

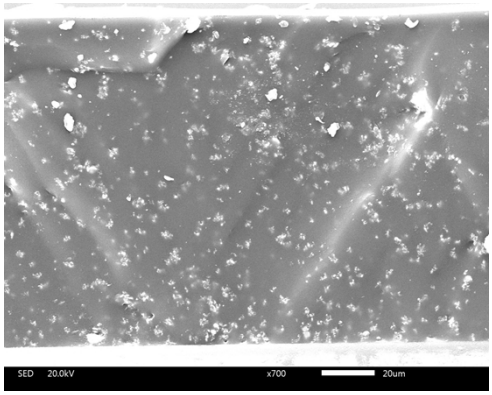

Figure S5 Cross-sectional SEM image of EGaIn NPs/PDMS-based photoacoustic

Role of different stabilizers on PA transducer

Fig. S6 shows optical microscope images of photoacoustic transducers prepared using LMNPs stabilized with two different surfactants: MPTMS and 1-octadecanethiol. As shown in Fig. S4(b), the silver-white dots indicate larger aggregates of liquid metal at the bottom of the transducer film when 1-octadecanethiol is used. These results demonstrate that MPTMS provides superior stabilization for the preparation of LMNP-based photoacoustic transducers.

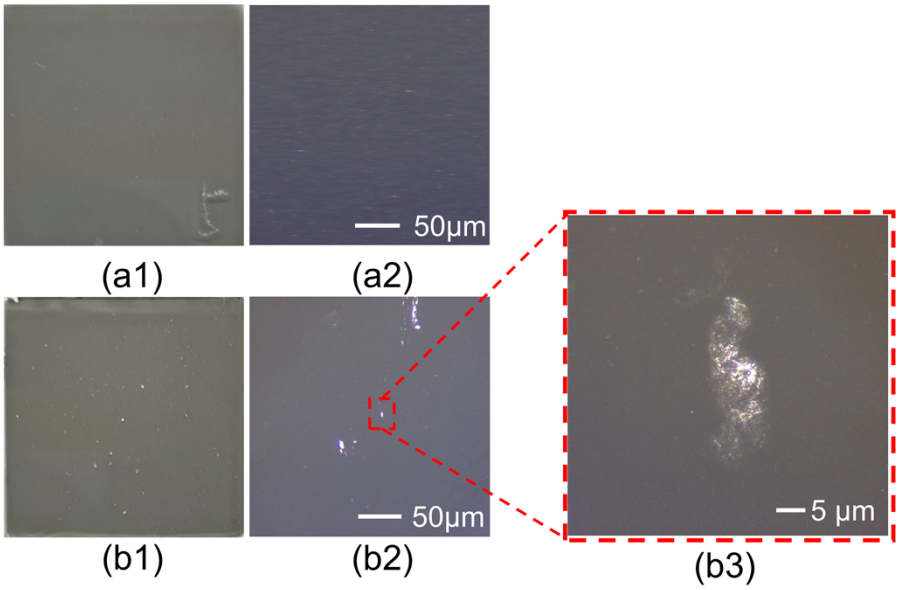

Figure S6 Optical microscope images of transducers prepared with different stabilizers: (a) MPTMS and (b) 1-octadecanethiol.

Simulated optical absorption of photoacoustic transducers with different size distribution of LMNPs

Fig. S7 demonstrates the simulation results of absorption variations induced by distinct particle size distributions, achieved under the condition of a constant total particle volume (with the weight ratio of LMNPs to PDMS remaining unchanged). Adjust the particle distribution and size parameters in the model according to the needs of this paper. The Gaussian distribution center particles are set up as D50, and the size of the nanoparticle clusters is set by setting the range of the spatial distribution of the particles, and the PDMS environment is used around the particles to approximate the real application external conditions. The results demonstrate that, under a fixed LMNPs/PDMS weight ratio, smaller particle sizes lead to a higher particle population density, thereby significantly enhancing the optical absorption capacity of the composite material

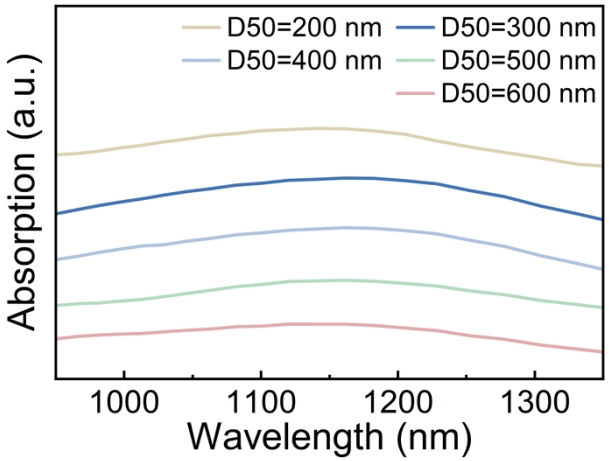

Figure S7 Simulated optical absorption of PA transducer with different D50 of LMNPs

Thermal diffusion and thermal expansion of transducer film with different mass ratios of LMNPs

Table S1 summarizes the thermal diffusion and thermal expansion coefficients of transducer films measured using TMA202 and LFA. As the mass fraction of LMNPs increases, the thermal expansion coefficient decreases, while the thermal diffusion coefficient increases.

Table S1 Thermal diffusion and thermal expansion characterization of PA transducer film

LMNPs mass radio (wt%)	Thermal diffusion (mm^2/s)	Thermal expansion (1/K)
8	0.062	6.66×10^{-4}
15	0.066	5.78×10^{-4}
20	0.073	4.95×10^{-4}

Simulated acoustic pressure from photoacoustic transducers with different mass ratios of LMNPs

Combining experimental data on optical absorption, thermal diffusion, and thermal expansion, a finite element simulation model was used to calculate the acoustic pressure generated by photoacoustic transducers with different LMNP mass ratios. As shown in Fig. S8, the transducer containing 15 wt% LMNPs achieves the highest acoustic pressure.

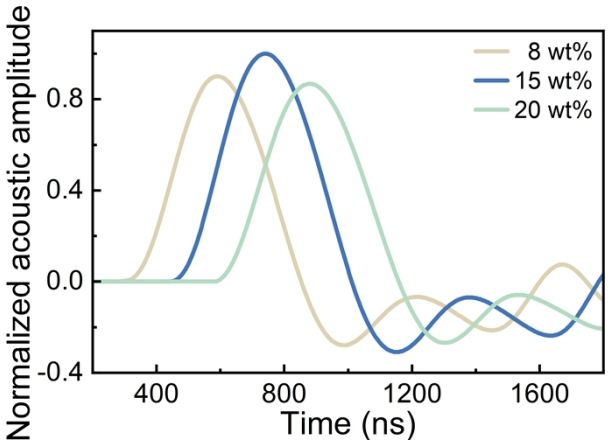

Figure S8 Simulated acoustic pressure from transducers with different LMNP mass ratios.

Performance Comparison of metal-based Photoacoustic Transducer Prepared from Different Materials

Table S2 showing the performance comparison of metal-based photoacoustic transducer prepared from different materials. The acoustic pressure and photoacoustic conversion efficiencies obtained in this work so far are the highest, and that the acoustic pressure is the largest, and it also shows that the transducer proposed in this paper is able to withstand higher energies.

Table S2 Performance Comparison of a Photoacoustic Transducer Prepared from Different Materials

Materials	Energy Density (mJ/cm^2)	Peak Pressure (MPa)	Efficiency ($\times 10^{-3}$)	Reference
AuNPs	13	0.189	0.022	[15]
Two-dimensional Au-nanostructure	0.004	0.002	/	[17]
Two-dimensional Au-nanostructure with a thin Au film	26	0.5	0.3	[18]
Cr thin film	2.35	1.82	0.42	[19]
AuNPs	8.75	0.64	0.18	[20]
EGaIn NP	300	21	5.01	This work

Experimental characterization results of planar and focused PA transducers

Fig. S9 compares the time-domain acoustic pressure generated by planar and focused PA transducers. The focused transducer demonstrates the ability to generate high acoustic pressure under low laser energy excitation.

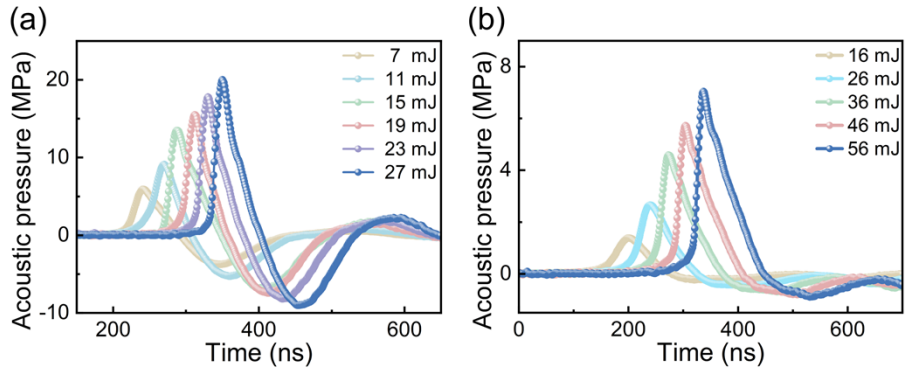

Figure S9 Time-domain acoustic pressure comparison of (a) Focused PA transducers (b) planar PA transducers.